

Article

# Wavefront Shaping by a Small-Aperture Deformable Mirror in the Front Stage for High-Power Laser Systems

Sensen Li <sup>1,2,\*</sup>, Luoxian Zhou <sup>2</sup>, Can Cui <sup>2</sup>, Kai Wang <sup>1</sup>, Xiusheng Yan <sup>1</sup>, Yirui Wang <sup>2</sup>, Lei Ding <sup>3</sup>, Yulei Wang <sup>2</sup> and Zhiwei Lu <sup>2</sup>

<sup>1</sup> Science and Technology on Electro-optical Information Security Control Laboratory, Tianjin 300308, China; wking\_man@yeah.net (K.W.); yanxs686@163.com (X.Y.)

<sup>2</sup> National Key Laboratory of Science and Technology on Tunable Laser, Harbin Institute of Technology, Harbin 150080, China; zhou185783806@163.com (L.Z.); cuicanzz.hit@gmail.com (C.C.); wangyiruibest@163.com (Y.W.); wyl@hit.edu.cn (Y.W.); zw\_lu@sohu.com (Z.L.)

<sup>3</sup> Research Center of Laser Fusion, China Academy of Engineering Physics, Mianyang 621900, China; dingleigongyong@126.com

\* Correspondence: sensli@163.com; Tel.: +86-186-9807-0942

Academic Editor: Christophe Finot

Received: 2 March 2017; Accepted: 10 April 2017; Published: 11 April 2017

**Abstract:** We demonstrate a method for wavefront distribution compensation with a low-cost small-aperture deformable mirror in the front stage of a complex high-power solid-state laser system. Meanwhile, an iterative algorithm for improving wavefront quality is indicated. Using this method, the wavefront compensation was studied in our single-shot high-power laser system that operated with and without the main amplifiers, respectively. The wavefront was compensated effectively, showing the near-flopped-shape output with the peak-to-valley value of  $0.29 \lambda$  and root mean square (RMS) of  $0.06 \lambda$  at 1053 nm.

**Keywords:** adaptive optics; deformable mirror; wavefront shaping; high-power laser

## 1. Introduction

High-power laser is of great interest for inertial confinement fusion [1–3], industrial processing [4,5], optoelectronic countermeasures [6], strong-field physics [7,8], and scientific research [9–12]. As an important factor related to the beam quality, a uniform wavefront is conducive to maintaining the high quality spatial distribution in propagation. The wavefront is directly related to the far-field distribution of the output laser that influences the focused intensity as well as the alignment of the beam path in a high-power laser system (like spatial filter) [13]. Additionally, in a frequency conversion module, the frequency conversion efficiency decreases sharply with the increase of the wavefront error [14,15], due to the angle matching of conversion cannot be achieved perfectly in the full aperture range. Therefore, it is necessary to control the wavefront in high-power laser systems, which can satisfy the basic requirements for laser transmission, focusing, and frequency conversion [16,17]. However, the factors causing wavefront distortion are various such as heat dissipation in gain medium and machining error of optical elements that are difficult to be suppressed, especially in a complex high-power laser system. At present, the wavefront compensation technique is an effective approach to improve the output beam quality.

Some devices have recently been employed for wavefront correction in high-power laser systems, and include stimulated Brillouin scattering phase conjugation mirrors (SBS-PCMs) [18–22], a liquid-crystal spatial light modulator (SLM) [23], and a deformable mirror (DM) [24–26]. Using SBS-PCMs is a passive method for wavefront shaping, and they are used as cavity end mirrors

that can only compensate the wavefront aberration of the elements in a double-pass structure. Unlike SBS-PCMs, SLMs and DMs are active devices for wavefront shaping. However, the maximum wavefront correction provided by an SLM is limited in  $2\pi$ , which cannot correct the large wavefront error in complex high-power lasers. Compared with SLMs, commercially available DMs are capable of wavefront correction with an adjustment range of up to several or even tens of micrometers [27,28]. Therefore, DMs are considered to be promising for correcting the low-frequency and large-area spatial wavefront distortion in a complex high-power laser system. To date, large-aperture DMs have been applied to wavefront shaping in many large solid-state laser systems, such as the National Ignition Facility in the Lawrence Livermore National Lab [29,30], the OMEGA EP Laser Facility at the University of Rochester [31,32], the LMJ Facility in France [33], and the SG-III Laser Facility in China [34,35]. Photo-controlled DMs are used in the HiLASE system at the Institute of Physics ASCR in Czech Republic [9,10,36–38]. These large-aperture DMs are placed in the end-stage of the laser systems to realize the wavefront compensation, which requires high-level machining technology and high cost. In addition, a higher risk of laser-induced damage may be introduced when a DM is exposed at the end of the high-power laser system with high fluence.

To address this challenge, we propose low-cost active wavefront shaping by placing a small-aperture DM at the front end of a high-power laser system. Different from the output-stage wavefront compensation by directly correcting the final output, our method realizes output wavefront optimization by pre-compensating the wavefront distortion by inserting an actively adjusting small-aperture reflecting DM in the front stage of the laser system. Through the feedback of iterative calculation, a high-quality flattening output wavefront can be effectively obtained. The rest of the paper is arranged as follows: Section 2 introduces the method of wavefront compensation for the entire laser system, Section 3 introduces the experimental setup, Section 4 presents the results of wavefront compensation both with and without the main amplifiers, respectively, and Section 5 draws the conclusion.

## 2. The Method of Wavefront Shaping

As shown in Figure 1, the initial wavefront distribution of the input laser beam can be expressed by  $\varphi_{\text{in}}(x, y)$ . The input beam is reflected by the DM and then passes through the laser system and arrives at the wavefront measurement system at the end. The output wavefront distribution expressed by  $\varphi_{\text{out}}(x, y)$  can be accurately measured by a Shack–Hartmann wavefront sensor. The formula for the entire process is depicted as follows:

$$\varphi_{\text{in}}(x, y) + 2S_{\text{DM}}(x, y) + F(x, y) = \varphi_{\text{out}}(x, y) \quad (1)$$

where  $S_{\text{DM}}(x, y)$  is the surface distribution of the DM, and  $F(x, y)$  is the wavefront distortion caused by the laser system. There are several factors affecting the low-frequency wavefront distortion in the laser system [39], including (1) the low-frequency surface distortion of the reflecting mirror; (2) wavefront distortion caused by the transmission through optical elements such as polarizer and window; (3) pumped dynamic thermal distortion and residual heat; (4) the spherical aberration and eccentric coma; and (5) air turbulence. The latter factor has the least influence on the system because of the random deformation. Under the wavefront distortion caused by the first four factors, the relationship can be seen as linear between the input wavefront and the output wavefront through the laser system. In order to study the closed-loop control of the output wavefront, the input wavefront distribution and the distortion caused by the laser system are merged into a transmission function expressed as

$$H(x, y) = \varphi_{\text{in}}(x, y) + F(x, y). \quad (2)$$

Under the initial case, the transmission function  $H(x, y)$  can be calculated from the initial output wavefront  $\varphi_{\text{out}}^{(0)}(x, y)$  and the DM surface  $S_{\text{DM}}^{(0)}(x, y)$ . The first compensation DM surface distribution

$S_{DM}^{(1)}(x, y)$  used for wavefront shaping in the laser system can be calculated from the aimed wavefront distribution  $\varphi_{aim}(x, y)$  and the transmission function  $H(x, y)$ . The formulas are as follows:

$$\begin{cases} H(x, y) = \varphi_{out}^{(0)}(x, y) - 2S_{DM}^{(0)}(x, y) \\ S_{DM}^{(1)}(x, y) = \frac{1}{2}[\varphi_{aim}(x, y) - H(x, y)] \end{cases} \quad (3)$$

The laser system itself (i.e., the aberrations) is actually linear, but the mirror actuators may not be. Thus, the output flattening wavefront distribution cannot be achieved after the first wavefront compensation. Under the circumstances, the iterative method is used for wavefront shaping [40]. The iterative format is as follows:

$$S_{DM}^{(n+1)}(x, y) = \frac{1}{2}[\varphi_{aim}(x, y) - \varphi_{out}^{(n)}(x, y)] + S_{DM}^{(n)}(x, y) \quad (4)$$

where  $S_{DM}^{(n)}(x, y)$  represents the DM surface distribution at the  $n$ -th iteration, and  $n = 0$ , the initial DM surface.  $\varphi_{out}^{(n)}(x, y)$  represents the  $n$ -th output wavefront distribution, and  $n = 0$ , the initial wavefront.

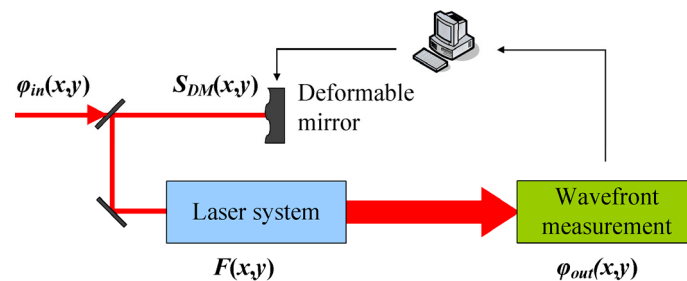


**Figure 1.** The structure of the wavefront shaping system. It consists of a small-aperture deformable mirror (DM), a laser system, and wavefront measurement (i.e., Shack–Hartmann wavefront sensor).

### 3. Experimental Setup

The wavefront distortion caused by the whole laser system is considered in the wavefront compensation by using the small-aperture DM in the front stage of the high-power laser system (see Figure 2). In the laser system, the pulse seeds generated from the all-fiber structure front end with 10 nJ/3 ns at the wavelength of 1053 nm [41] passes through the preamplifier providing a high gain of  $10^5$  times, and its output energy reaches a 200  $\mu$ J level after the beam shaper. The beam shaper mainly compensates the spatial intensity of the output laser to achieve a high-quality nearfield. A four-stage Nd/glass rod amplifier is applied in the laser system with an output energy of 100 J and a beam diameter of  $D = 60$  mm at the end [42,43]. In the complex laser system with a low operating repetition rate of approximately 2 shots per hour, an electricity-controlled DM is used for adaptive wavefront shaping. The electromagnetic DM (Imagine Eyes, Mirao-52e) is arranged as the cavity mirror ( $0^\circ$  reflection) of the two-pass  $\Phi 20$  mm Nd/glass amplifier, which relatively easily calculates the DM surface to correct the wavefront distortion in the closed loop. The overall aperture of the DM is 15 mm, which matches the 13 mm beam aperture in the beam pass of the first main amplifier. The fluence is low ( $<0.01$  J/cm $^2$ ) at the cavity mirror position of the first amplifier. The DM we adopted is an active wavefront-shaping device with 52 motors providing a continuously deformable surface within a range of  $\pm 50$   $\mu$ m. The sensitivity is about 0.02  $\mu$ m RMS, which is acceptable with this device. It can compensate the wavefront distortion caused by the following amplification and transmission. The Shack–Hartmann wavefront sensor (Thorlabs WFS150-5C) is placed at the end to measure the output wavefront distribution. The cavity mirror position is the image relay plane. The DM and the Shack–Hartmann wavefront sensor are both at the image-conjugate-plane. Indeed, the DM mainly corrects the wavefront of the image-conjugate plane in the laser system.

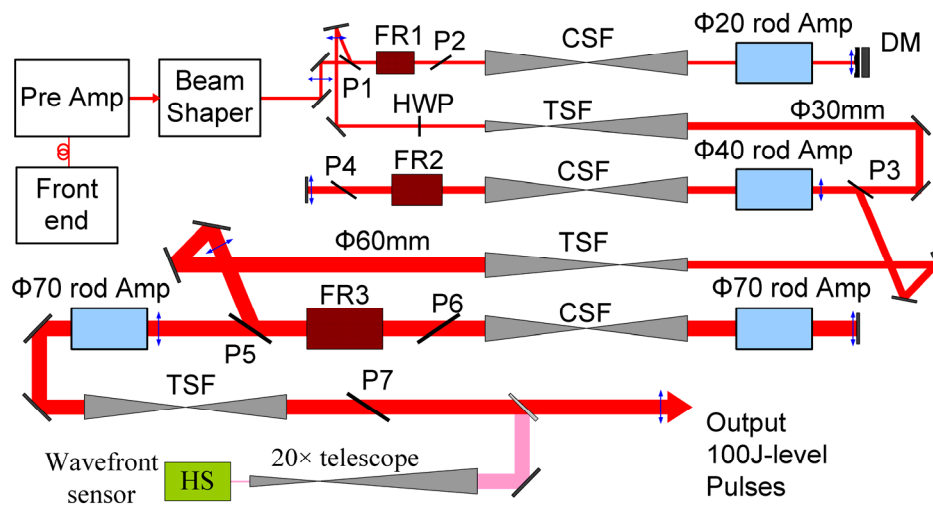


**Figure 2.** Overview of the wavefront shaping system in the laser system. The complex laser system consists of an all-fiber front end, a preamplifier, a transmission and amplifier, a frequency converter, and beam control and measurement. The blue two-direction arrow real lines refer to the relay image plane. P1 to P7: polarizers; FR1 to FR3: Faraday rotators; DM: deformable mirror; HWP: half-wave plate; CSF: cavity spatial filter in the main amplifier system; TSF: transport spatial filter;  $\Phi 20$ ,  $\Phi 40$ , and  $\Phi 70$  rod Amp: 20, 40, and 70-mm-diameter Nd/phosphate glass rod amplifiers; the bidirectional blue arrow: the image relay plane.

We assume that an additional compensation of aberration is obtained by adjusting the position of a spatial filter lens, so the DM can be used alone. Before wavefront shaping, the beam alignment is finished and the beam passes through a series of spatial filter pinholes successfully. A laser spot angular radius at 99% of energy in the pinhole planes of the spatial filters are calculated in order to be compared with the pinhole dimensions. The laser spot angular radius is less than a 3.5 diffraction limit (DL). These pinhole radii are equal to 7.5–30 DL (pinhole size is nearly 2~2.5 mm). Indeed, the laser can pass through the pinholes without clipping at the pinholes.

In this experiment, for the wavefront compensation without the main amplifiers in operation, the preamplifier operates at 1 Hz. When the DM works in a closed loop, it needs about 2 min to perform a one closed-loop operation to finish the calculation and uploading data. For wavefront compensation with the main amplifiers in operation, the interval between system shots is 30 min. Before wavefront shaping, the near-field fluence of the output laser has been shaped to be flat-top [44–46]. The stable near-field output is a necessary condition for good wavefront correction.

## 4. Experimental Results and Discussion

### 4.1. Wavefront Compensation without the Main Amplifiers in Operation

Before wavefront shaping, the DM surface is set so that the beam can pass through the pinhole of spatial filter. Firstly, without the operation of the main amplifiers, the wavefront distortion of the entire laser system is observed when the DM is not working. At this condition, a plane  $0^\circ$  reflection mirror is placed at the DM position as the cavity mirror of the two-pass  $\Phi 20$  Nd/glass rod amplifier. Here, the wavefront refers to the output wavefront measured by the wavefront sensor in the diagnostic system when a pulse seed passes through the entire laser system without the main amplifiers working. Figure 3a shows the output wavefront distribution without the DM work. The saddle-shaped wavefront distribution indicates that the astigmatism aberration is very distinct in the laser system. The calculated wavefront peak-to-valley (PV) value is  $3.34 \lambda$  ( $\lambda = 1053 \text{ nm}$ ) and the RMS value (i.e., root mean square) is  $0.65 \lambda$ . Obviously, it is necessary to do wavefront shaping to compensate the wavefront distortion without the main amplifiers in operation in the laser system.

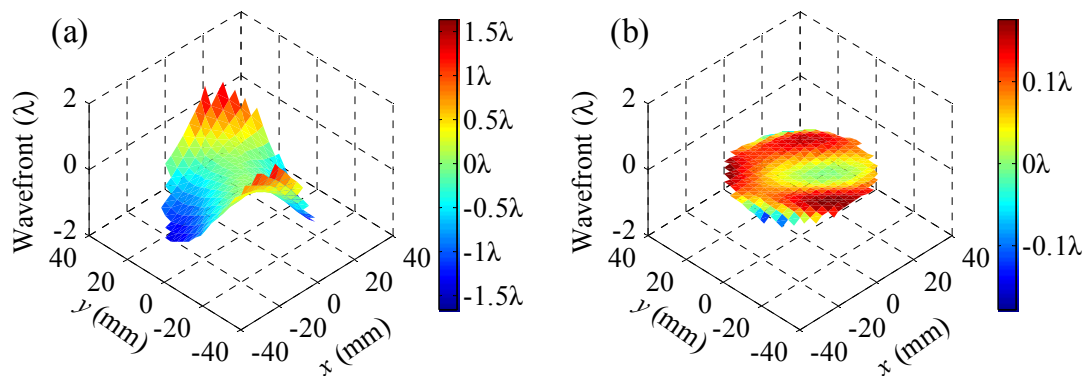


**Figure 3.** The output wavefront during the process of wavefront compensation without the main amplifiers in operation. (a) The output wavefront without DM; (b) the final output.

After the DM is installed in the beamline instead of the cavity mirror of the two-pass  $\Phi 20$  rod amplifier, the output wavefront without the main amplifiers in operation can be shaped actively. An off-line well-corrected DM surface is set to observe the initial output wavefront distribution with a PV value of  $2.29 \lambda$  and an RMS value of  $0.51 \lambda$ . It is also the saddle-shaped distribution in the whole beam. According to the wavefront shaping method introduced in Section 2, the output wavefront distribution tends to flatten after the first compensation. After several iterations of compensation, the wavefront distribution gradually tends to flatten more; the final output wavefront PV value is  $0.36 \lambda$ , and the RMS value is  $0.06 \lambda$  (see Figure 3b). The wavefront shaping algorithm is effective in realizing the wavefront shaping without the main amplifiers in operation in the laser system. Figure 4 indicates that both the PV and RMS values of the output wavefront decrease obviously in the entire shaping process. During the first three shots, the output wavefront changes greatly and then changes relatively slowly against the laser shot number as well as the increasing iteration times.

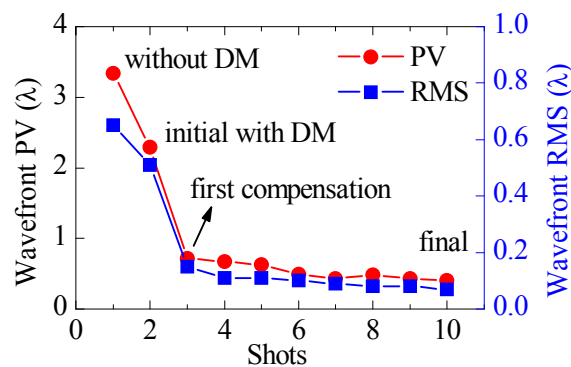


**Figure 4.** The wavefront variety during the process of wavefront compensation without the main amplifiers in operation.

After wavefront compensation without the main amplifiers in operation, the PV value of the output wavefront is less than  $0.5 \lambda$ , and the beam passes through the laser system successfully. The wavefront distortions without the main amplifiers in operation here mainly result from the original beam distortion of the pulse seed and the imperfections in a series of optical components in the laser system. These distortions have been compensated by the DM. Because the anisotropic thermal dissipation in the amplification media caused by the main amplifiers involves a deterioration of the wavefront profile as the laser system operates at a high energy level, a further wavefront shaping with the main amplifiers in operation is needed based on this work.

#### 4.2. Wavefront Compensation with the Main Amplifiers in Operation

Depending on the perfect DM surface achieved in the wavefront compensation experiment without the main amplifiers in operation, the output wavefront with the main amplifiers in operation is measured when the laser system operates at a 40 J level with a 3 ns pulse duration, as an example. Figure 5a shows that the initial output wavefront distribution with a PV value of  $0.86 \lambda$  and an RMS value of  $0.14 \lambda$ . This wavefront is not as good as the one without the main amplifiers in operation, because of the wavefront distortion of the pumped dynamic thermal distortion and residual heat in the laser system. Therefore, it is necessary to compensate the distortion by the wavefront shaping method introduced in Section 2. In terms of this experiment, the laser system operates at a single-shot low repetition rate of approximately 2 shots per hour. As the iterative times increase in the following several shots, the output wavefront tends to flatten. In the wavefront shaping process, the best wavefront distribution of the final output laser is shown in Figure 5b with a PV value of  $0.29 \lambda$  and an RMS value of  $0.06 \lambda$ , respectively.

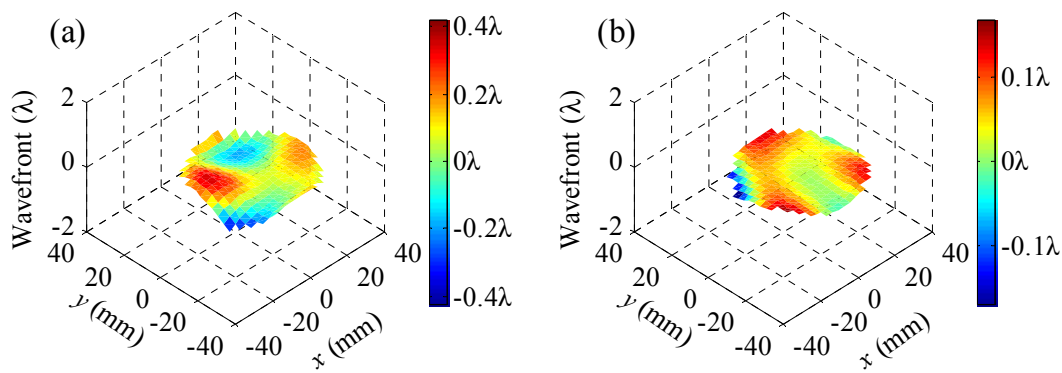


**Figure 5.** The output wavefront of the wavefront shaping with the main amplifiers in operation. (a) The initial output with DM; (b) the final output.

The flattening wavefront distribution is achieved after the wavefront shaping by using the front-stage small-aperture DM in the high-power laser system. Figure 6 shows the output wavefront PV and RMS value change in the shaping process. Based on several iterations compensation, the output wavefront is corrected to flatten with a PV value of less than  $0.4 \lambda$  and an RMS value of about  $0.06 \lambda$ , respectively. As a whole, with the increase in the iterative time, the PV and RMS values gradually decrease. When the PV value is small enough (less than  $0.5 \lambda$ ), with the increase in iterative time, the output wavefront PV and RMS values have a slight fluctuation, which is caused by the randomness of the dynamic wavefront distortion and operation stability of the high-power laser system.

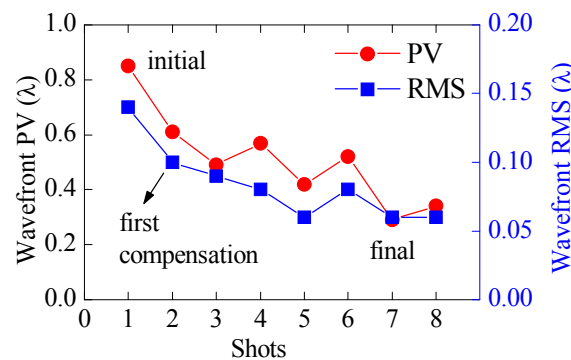


**Figure 6.** The output wavefront PV and RMS values during the process of wavefront compensation with the main amplifiers in operation.

From the results of the wavefront-shaping experiment, the output wavefront can be achieved as the flattening distribution by the wavefront compensation without the main amplifiers in operation, but the output wavefront with the main amplifiers in operation is not necessarily good because of the wavefront distortion caused by the main amplifiers. By wavefront shaping with the main amplifiers in operation, the output wavefront meets the expectation with a PV value of less than  $0.4 \lambda$ . The 1053 nm flattening wavefront laser can be injected into the frequency conversion module of the high-power laser system for the third harmonic generation.

## 5. Conclusions

In summary, we report here a wavefront beam shaping technique for a high-power laser system by utilizing the measured wavefront with a Shack–Hartmann wavefront sensor at the output of the system as feedback to control the small-aperture DM at the front stage. A closed-loop algorithm is proposed in controlling the motors inside the DM to correct the wavefront distortion. Finally, the output wavefront is successfully shaped to be flat by using this approach, with the output PV value improved from  $3.34 \lambda$  to  $0.29 \lambda$  and the RMS value improved from  $0.65 \lambda$  to  $0.06 \lambda$  at 1053 nm. This method shows great potential for wavefront shaping in a complex high-power laser system with low cost and high efficiency.

**Acknowledgments:** The authors appreciate the efforts of Meng Xia, Xi Chen, Dexin Ba, and Xin Wang from the Harbin Institute of Technology, who have been instrumental in the success of this project. This work is supported by the project of the National Natural Science Foundation of China (NSFC) under Grant No. 61622501. The support does not constitute an endorsement by the NSFC of the views expressed in this article.

**Author Contributions:** The experiments were done by Sensen Li, Luoxian Zhou, and Can Cui. Kai Wang, Xiusheng Yan, and Yirui Wang contributed to the data analysis and the discussion of the results. Lei Ding participated in research plan development. Zhiwei Lu and Yulei Wang conceived and supervised this work. Sensen Li wrote the paper with contribution from all authors.

**Conflicts of Interest:** The authors declare no conflict of interest.

## References

1. Moses, E.I. Ignition on the National Ignition Facility: A path towards inertial fusion energy. *Nucl. Fusion* **2009**, *49*, 104022. [[CrossRef](#)]
2. Obenschain, S.; Lehmberg, R.; Kehne, D.; Hegeler, F.; Wolford, M.; Sethian, J.; Weaver, J.; Karasik, M. High-energy krypton fluoride lasers for inertial fusion. *Appl. Opt.* **2015**, *54*, 103–122. [[CrossRef](#)] [[PubMed](#)]
3. Edwards, C.B.; Danson, C.N. Inertial confinement fusion and prospects for power production. *High Power Laser Sci. Eng.* **2015**, *3*, e4. [[CrossRef](#)]
4. Beck, R.J.; Parry, J.P.; MacPherson, W.N.; Waddie, A.; Weston, N.J.; Shephard, J.D.; Hand, D.P. Application of cooled spatial light modulator for high power nanosecond laser micromachining. *Opt. Express* **2010**, *18*, 17059–17065. [[CrossRef](#)] [[PubMed](#)]
5. Bai, Z.; Cui, C.; Liu, Z.; Yuan, H.; Wang, H.; Wang, Y.; Lu, Z. Drilling study on Cu, Mo, W and Ti by using SBS pulse compressed steep leading edge hundred picoseconds laser. *Optik* **2016**, *127*, 11156–11160. [[CrossRef](#)]
6. Elder, I. Performance requirements for countermeasures lasers. *Proc. SPIE* **2010**, 7836, 783605.
7. Remo, J.L.; Adams, R.G. High energy density laser interactions with planetary and astrophysical materials: methodology and data. *Proc. SPIE 7005 High-Power Laser Ablation VII* **2008**, 7005. [[CrossRef](#)]
8. Liu, J.; Wang, W.; Wang, Z.; Lv, Z.; Zhang, Z.; Wei, Z. Diode-pumped high energy and high average power all-solid-state picosecond amplifier systems. *Appl. Sci.* **2015**, *5*, 1590–1602. [[CrossRef](#)]
9. Divoky, M.; Smrz, M.; Chyla, M.; Sikocinski, P.; Severova, P.; Novak, O.; Huynh, J.; Nagisetty, S.; Miura, T.; Pilař, J. Overview of the HiLASE project: high average power pulsed DPSSL systems for research and industry. *High Power Laser Sci. Eng.* **2014**, *2*, e14. [[CrossRef](#)]
10. Novák, O.; Miura, T.; Smrž, M.; Chyla, M.; Nagisetty, S.S.; Mužík, J.; Linnemann, J.; Turčičová, H.; Jambunathan, V.; Slezák, O. Status of the high average power diode-pumped solid state laser development at HiLASE. *Appl. Sci.* **2015**, *5*, 637–665. [[CrossRef](#)]

11. Bai, Z.; Wang, Y.; Lu, Z.; Yuan, H.; Zheng, Z.; Li, S.; Chen, Y.; Liu, Z.; Cui, C.; Wang, H.; Liu, R. High compact, high quality single longitudinal mode hundred picoseconds laser based on stimulated brillouin scattering pulse compression. *Appl. Sci.* **2016**, *6*, 29. [[CrossRef](#)]
12. Yu, M.; Hu, G.; An, N.; Qian, F.; Wu, Y.; Zhang, X.; Gu, Y.; Wang, Q.; Zheng, J. Hard X-ray transmission curved crystal spectrometers (10–100 keV) for laser fusion experiments at the ShenGuang-III laser facility. *High Power Laser Sci. Eng.* **2016**, *4*, e2. [[CrossRef](#)]
13. Kruschwitz, B.; Bahk, S.-W.; Bromage, J.; Moore, M.; Irwin, D. Accurate target-plane focal-spot characterization in high-energy laser systems using phase retrieval. *Opt. Express* **2012**, *20*, 20874–20883. [[CrossRef](#)] [[PubMed](#)]
14. Barker, C.E.; Auerbach, J.M.; Adams, C.H.; Bumpas, S.E.; Hibbard, R.; Lee, C.S.; Roberts, D.; Campbell, J.H.; Wegner, P.J.; Van Wonterghem, B.M. National Ignition Facility frequency converter development. *Proc. SPIE* **1997**, *3047*, 197–202.
15. Auerbach, J.M.; Wegner, P.J.; Couture, S.A.; Eimerl, D.; Hibbard, R.L.; Milam, D.; Norton, M.A.; Whitman, P.K.; Hackel, L.A. Modeling of frequency doubling and tripling with measured crystal spatial refractive-index nonuniformities. *Appl. Opt.* **2001**, *40*, 1404–1411. [[CrossRef](#)] [[PubMed](#)]
16. Schwarz, J.; Ramsey, M.; Smith, I.; Headley, D.; Porter, J. Low order adaptive optics on Z-Beamlet using a single actuator deformable mirror. *Opt. Commun.* **2006**, *264*, 203–212. [[CrossRef](#)]
17. Kasprzack, M.; Canuel, B.; Cavalier, F.; Day, R.; Genin, E.; Marque, J.; Sentenac, D.; Vajente, G. Performance of a thermally deformable mirror for correction of low-order aberrations in laser beams. *Appl. Opt.* **2013**, *52*, 2909–2916. [[CrossRef](#)] [[PubMed](#)]
18. Kuzmin, A.A.; Khazanov, E.A.; Kulagin, O.V.; Shaykin, A.A. Neodymium glass laser with a phase conjugate mirror producing 220 J pulses at 0.02 Hz repetition rate. *Opt. Express* **2014**, *22*, 20842–20855. [[CrossRef](#)] [[PubMed](#)]
19. Kong, H.J.; Park, S.; Cha, S.; Ahn, H.; Lee, H.; Oh, J.; Lee, B.J.; Choi, S.; Kim, J.S. Conceptual design of the Kumgang laser: A high-power coherent beam combination laser using SC-SBS-PCMs towards a dream laser. *High Power Laser Sci. Eng.* **2015**, *3*, e1. [[CrossRef](#)]
20. Dane, C.; Zapata, L.; Neuman, W.; Norton, M.; Hackel, L. Design and operation of a 150 W near diffraction-limited laser amplifier with SBS wavefront correction. *IEEE J. Quantum Electron.* **1995**, *31*, 148–163. [[CrossRef](#)]
21. Dane, C.B.; Hackel, L.A.; Halpin, J.M.; Daly, J.; Harrisson, J.; Harris, F.B., Jr. High-throughput laser peening of metals using a high-average-power Nd: Glass laser system. *Proc. SPIE* **2000**, *3887*, 211–221.
22. Kalal, M.; Kong, H.J.; Slezak, O.; Koresheva, E.R.; Park, S.; Startsev, S.A. Recent progress made in the SBS PCM approach to self-navigation of lasers on direct drive IFE targets. *J. Fusion Energy* **2010**, *29*, 527–531. [[CrossRef](#)]
23. Bahk, S.-W.; Fess, E.; Kruschwitz, B.E.; Zuegel, J.D. A high-resolution, adaptive beam-shaping system for high-power lasers. *Opt. Express* **2010**, *18*, 9151–9163. [[CrossRef](#)] [[PubMed](#)]
24. Liao, Z.M. *Initial Demonstration of Mercury Wavefront Correction System*; Report UCRL-TR-218721; Lawrence Livermore National Laboratory (LLNL): Livermore, CA, USA, 2006.
25. Canova, F.; Flacco, A.; Canova, L.; Clady, R.; Chambaret, J.-P.; Ple, F.; Pittman, M.; Planchon, T.; Silva, M.; Benocci, R. Efficient aberrations pre-compensation and wavefront correction with a deformable mirror in the middle of a petawatt-class CPA laser system. *Laser Part. Beams* **2007**, *25*, 649–655. [[CrossRef](#)]
26. Dong, B.; Li, Y.; Han, X.-L.; Hu, B. Dynamic aberration correction for conformal window of high-speed aircraft using optimized model-based wavefront sensorless adaptive optics. *Sensors* **2016**, *16*, 1414. [[CrossRef](#)] [[PubMed](#)]
27. Devaney, N.; Dalimier, E.; Farrell, T.; Coburn, D.; Mackey, R.; Mackey, D.; Laurent, F.; Daly, E.; Dainty, C. Correction of ocular and atmospheric wavefronts: A comparison of the performance of various deformable mirrors. *Appl. Opt.* **2008**, *47*, 6550–6562. [[CrossRef](#)] [[PubMed](#)]
28. Florentin, R.; Kermene, V.; Benoist, J.; Desfargesberthelemot, A.; Pagnoux, D.; Barthélémy, A.; Huignard, J.P. Shaping the light amplified in a multimode fiber. *Light Sci. Appl.* **2017**, *6*, e16208. [[CrossRef](#)]
29. Zacharias, R.; Bliss, E.; Winters, S.; Sacks, R.A.; Feldman, M.; Grey, A.; Koch, J.A.; Stolz, C.J.; Toeppen, J.S.; Van Atta, L. Wavefront control of high-power laser beams in the National Ignition Facility (NIF). *Proc. SPIE* **2000**, *3889*, 332–343.

30. Zacharias, R.A.; Beer, N.R.; Bliss, E.S.; Burkhart, S.C.; Cohen, S.J.; Sutton, S.B.; Van Atta, R.; Winters, S.E.; Salmon, J.T.; Latta, M.R. Alignment and wavefront control systems of the National Ignition Facility. *Opt. Eng.* **2004**, *43*, 2873–2884. [[CrossRef](#)]
31. Waxer, L.; Maywar, D.; Kelly, J.; Kessler, T.; Kruschwitz, B.; Loucks, S.; McCrory, R.; Meyerhofer, D.; Morse, S.; Stoeckl, C. High-energy petawatt capability for the OMEGA laser. *Opt. Photonics News* **2005**, *16*, 30–36. [[CrossRef](#)]
32. Bromage, J.; Bahk, S.-W.; Irwin, D.; Kwiatkowski, J.; Pruyne, A.; Millecchia, M.; Moore, M.; Zuegel, J. A focal-spot diagnostic for on-shot characterization of high-energy petawatt lasers. *Opt. Express* **2008**, *16*, 16561–16572. [[PubMed](#)]
33. Mainguy, S.; Grosset-Grange, C.; Bordenave, E. Performance of a high-resolution deformable mirror for wavefront correction on the LIL/LMJ and PETAL baselines. *J. Phys. Conf. Ser.* **2010**, *244*, 032021. [[CrossRef](#)]
34. Wanjun, D.; Dongxia, H.; Wei, Z.; Junpu, Z.; Feng, J.; Zeping, Y.; Kun, Z.; Xuejun, J.; Wu, D.; Runchang, Z. Beam wavefront control of a thermal inertia laser for inertial confinement fusion application. *Appl. Opt.* **2009**, *48*, 3691–3694. [[CrossRef](#)] [[PubMed](#)]
35. Jing, F.; Dai, W.; Hu, D.; Wang, D.; Liu, L.; Zhou, W.; Zhang, X.; Deng, W.; Zhang, K. Beam wavefront correction scheme for application in a multi-pass amplifier system. In Proceedings of the Conference on Lasers and Electro-Optics/Pacific Rim, Sydney, Australia, 28 August–1 September 2011.
36. Divoky, M.; Sikocinski, P.; Pilar, J.; Lucianetti, A.; Sawicka, M.; Slezak, O.; Mocek, T. Design of high-energy-class cryogenically cooled Yb<sup>3+</sup>:YAG multislabs laser system with low wavefront distortion. *Opt. Eng.* **2013**, *52*, 064201. [[CrossRef](#)]
37. Pilar, J.; Slezak, O.; Sikocinski, P.; Divoky, M.; Sawicka, M.; Bonora, S.; Lucianetti, A.; Mocek, T.; Jelinkova, H. Design and optimization of an adaptive optics system for a high-average-power multi-slab laser (HiLASE). *Appl. Opt.* **2014**, *53*, 3255–3261. [[CrossRef](#)] [[PubMed](#)]
38. Lucianetti, A.; Sawicka, M.; Slezak, O.; Divoky, M.; Pilar, J.; Jambunathan, V.; Bonora, S.; Antipenkov, R.; Mocek, T. Design of a kJ-class HiLASE laser as a driver for inertial fusion energy. *High Power Laser Sci. Eng.* **2014**, *2*, e13. [[CrossRef](#)]
39. Williams, W.H.; Auerbach, J.M.; Henesian, M.A.; Lawson, J.K.; Hunt, J.T.; Sacks, R.A.; Widmayer, C.C. Modeling characterization of the National Ignition Facility focal spot. *Proc. SPIE* **1998**, *3264*, 93–104.
40. Haber, A.; Polo, A.; Smith, C.S.; Pereira, S.F.; Urbach, P.; Verhaegen, M. Iterative learning control of a membrane deformable mirror for optimal wavefront correction. *Appl. Opt.* **2013**, *52*, 2363–2373. [[CrossRef](#)] [[PubMed](#)]
41. Li, S.; Wang, Y.; Lu, Z.; Ding, L.; Chen, Y.; Du, P.; Ba, D.; Zheng, Z.; Wang, X.; Yuan, H.; et al. Hundred-Joule-level, nanosecond-pulse Nd:glass laser system with high spatiotemporal beam quality. *High Power Laser Sci. Eng.* **2016**, *4*, e10. [[CrossRef](#)]
42. Li, S.; Wang, Y.; Lu, Z.; Ding, L.; Chen, Y.; Du, P.; Zheng, Z.; Ba, D.; Yuan, H.; Zhu, C. Hundred-J-Level, Nanosecond-Pulse Nd: glass Laser System with High Beam Quality. In Proceedings of the European Conference on Lasers and Electro-Optics, Munich, Germany, 21–25 June 2015.
43. Wang, Y.; Liu, R.; Yuan, H.; Li, S.; Liu, Z.; Zhu, X.; He, W.; Lu, Z. Using an active temporal compensating system to achieve the super-Gaussian pulses in high-power lasers. In Proceedings of the SPIE, International Symposium on Photonics and Optoelectronics, Shanghai, China, 22 August 2015.
44. Li, S.; Wang, Y.; Lu, Z.; Ding, L.; Cui, C.; Chen, Y.; Pengyuan, D.; Ba, D.; Zheng, Z.; Yuan, H.; et al. Spatial beam shaping for high-power frequency tripling lasers based on a liquid crystal spatial light modulator. *Opt. Commun.* **2016**, *367*, 181–185. [[CrossRef](#)]
45. Ding, L.; Li, S.; Zhou, L.; Lu, Z.; Wang, Y.; Tan, T.; Yuan, H.; Bai, Z.; Cui, C. Study on near-field image extraction in high power lasers. *Optik* **2016**, *127*, 4495–4497. [[CrossRef](#)]
46. Li, S.; Wang, Y.; Lu, Z.; Ding, L.; Du, P.; Chen, Y.; Zheng, Z.; Ba, D.; Dong, Y.; Yuan, H. High-quality near-field beam achieved in a high-power laser based on SLM adaptive beam-shaping system. *Opt. Express* **2015**, *23*, 681–689. [[CrossRef](#)] [[PubMed](#)]

